photonics

IMPACT FACTOR 1.9

CITESCORE 3.5

Article

Entanglement Dynamics of Two Giant Atoms Embedded in a One-Dimensional Photonic Lattice with a Synthetic Gauge Field

Vassilios Yannopapas

Special Issue
Advanced Research in Quantum Optics

Edited by
Dr. Wei Li

MDPI

https://doi.org/10.3390/photonics12060612

photonics

MDPI

Article

Entanglement Dynamics of Two Giant Atoms Embedded in a One-Dimensional Photonic Lattice with a Synthetic Gauge Field

Vassilios Yannopapas

Department of Physics, School of Applied Mathematical and Physical Sciences, National Technical University of Athens, GR-15780 Athens, Greece; vyannop@mail.ntua.gr

Abstract: We investigate the entanglement dynamics of two giant atoms coupled to a one-dimensional photonic lattice with synthetic chirality. The atoms are connected to multiple lattice sites in a braided configuration and interact with a structured photonic reservoir featuring direction-dependent hopping phases. By tuning the atomic detuning and the synthetic gauge phase, we identify distinct dynamical regimes characterized by decoherence-free population exchange, damped oscillations, long-lived revivals, and excitation trapping. Using a combination of time-domain simulations and resolvent-based analysis, we show how interference and band structure effects lead to the emergence of bound states, quasi-bound states, and phase-dependent entanglement dynamics. We compare the initial states with localized and delocalized atomic excitations, demonstrating that pre-existing entanglement can enhance the robustness against decoherence or accelerate its loss, depending on the system parameters. These results highlight the utility of synthetic photonic lattices and nonlocal emitter configurations in tailoring quantum coherence, entanglement, and information flows in structured environments.

Keywords: giant atoms; non-Hermitian lattice; non-Markovian dynamics

Received: 29 May 2025
Revised: 8 June 2025
Accepted: 13 June 2025
Published: 14 June 2025

Citation: Yannopapas, V. Entanglement Dynamics of Two Giant Atoms Embedded in a One-Dimensional Photonic Lattice with a Synthetic Gauge Field. *Photonics* **2025**, *12*, 612. https://doi.org/10.3390/photonics12060612

1. Introduction

The interaction between quantum emitters and low-dimensional photonic environments has become a focal point in modern quantum optics, with waveguide quantum electrodynamics (QED) serving as a foundational theoretical framework [1–3]. Such systems enable precise control over light–matter coupling, which is essential in advancing quantum communication and computation platforms. Recent experimental progress has made it possible to fabricate engineered photonic reservoirs—including one-dimensional waveguides and photonic lattices—and couple them effectively to quantum emitters. Realizations across multiple platforms, such as optical photonic crystals [4], superconducting microwave circuits [5–7], and synthetic atomic systems [8,9], have expanded the scope of quantum photonics by uncovering novel mechanisms for the manipulation of quantum light.

Among these advances, the concept of the *giant atom* (GA) has emerged as a particularly compelling paradigm [10]. In contrast to conventional atoms, which couple locally to the electromagnetic field, GAs interact with the field at multiple points spaced by distances on the order of the wavelength. This spatially extended coupling introduces interference among different emission paths and leads to several unusual quantum-optical phenomena. Notable effects include frequency-dependent Lamb shifts and decay rates [11,12], decoherence-free interactions mediated through structured continua [13–18], and the emergence of bound or quasi-bound oscillatory states [19–23].

Experimentally, GAs have been successfully realized in a range of architectures. A particularly fruitful approach involves coupling superconducting qubits to surface acoustic waves [24–35] or to microwave transmission lines and waveguides [12,14,36]. These platforms offer fine control over the coupling geometry and interaction strength. Theoretical work has also expanded the range of possible GA implementations, including proposals for synthetic frequency dimensions [37] and on-chip photonic circuits [38]. More recently, the giant atom concept has been generalized to include large-scale quantum systems such as giant molecules [39–44] and collective spin ensembles [45].

Despite the diversity of platforms, most prior studies have concentrated on GAs coupled to continuum waveguides [11–14,16,18–20,22,36,42,46–61], where the photonic density of states varies slowly with the frequency. However, structured reservoirs—such as tight-binding photonic lattices—have recently gained increased interest for their rich dispersion properties and spectral features [17,23,38,42,52,62–83]. These reservoirs allow for the emergence of non-Markovian behavior, bound states in the continuum, and synthetic gauge effects.

In our previous work [84], where we studied the non-Markovian dynamics of a single giant atom (GA) coupled to a one-dimensional photonic lattice with synthetic chirality, we demonstrated that complex hopping phases and multi-point interference can yield a rich variety of light–matter interactions. In particular, we found that the synthetic gauge phase ϕ in the lattice governs directional emission asymmetry, decoherence-free subspaces, and the emergence of photonic bound states. An exact analytic expression for the self-energy revealed how spatially separated coupling points allow phase-tuned interference, resulting in long-lived coherence and partial entanglement [84]. These findings highlighted the potential of using geometry and synthetic phases to engineer emission dynamics and atom–bath correlations in structured photonic environments.

Here, we extend this framework to a system of two braided GAs symmetrically coupled to the same structured photonic lattice [16]. The multi-emitter configuration introduces new collective phenomena beyond those accessible with a single GA. Using a combination of resolvent analysis and time-domain simulations in the single-excitation subspace, we study how synthetic chirality, atomic detuning Δ, and spatial coupling geometry shape the dynamics of population exchange, atom–field entanglement, and von Neumann entropy. We observe a broad spectrum of behaviors—including decoherence-free interactions, non-Markovian revivals, quasi-bound states at the band edge, and complete excitation localization outside the band. Furthermore, by comparing initially unentangled and Bell-state-prepared atoms, we reveal how the initial correlations influence entanglement decay and robustness. These results advance the understanding of cooperative emitter dynamics in nonreciprocal environments and demonstrate how synthetic gauge control and spatial interference can be leveraged to design non-Markovian quantum interfaces [80,81,83].

2. Theory

2.1. Model and Hamiltonian

We consider two identical giant atoms (GAs), labeled A and B, each modeled as a two-level emitter with excited states $|e_A\rangle, |e_B\rangle$ and ground states $|g_A\rangle, |g_B\rangle$. The atoms interact with a one-dimensional tight-binding photonic lattice possessing synthetic chirality introduced by a complex hopping amplitude $Je^{\pm i\phi}$ [85] (see Figure 1). Each atom is coupled to P spatially separated lattice sites, located at positions $\{n_p^j = n_0^j + (p-1)d\}_{p=1}^{P}$ for $j = A, B$, where d is the separation between coupling points and $D = n_0^B - n_0^A$ is the center-to-center atom separation.

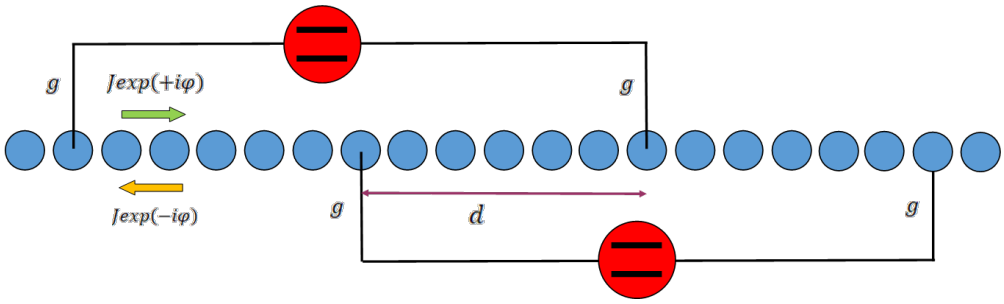

Figure 1. Schematic of the system under study: two braided giant atoms (red) are coupled to a one-dimensional photonic lattice (blue sites) at multiple spatially separated points. The lattice features complex hopping amplitudes $Je^{\pm i\phi}$ that induce synthetic chirality, enabling nonreciprocal photon propagation. Each atom couples to two sites (forming a four-point braided configuration), with inter-point coupling separation d. The parameter g denotes the atom–lattice coupling strength at each site.

The full Hamiltonian in a rotating frame with respect to the lattice band center is

$$H = \Delta \sum_{j=A,B} \sigma_j^\dagger \sigma_j + J \sum_n \left(e^{i\phi} a_n^\dagger a_{n+1} + e^{-i\phi} a_{n+1}^\dagger a_n \right) + g \sum_{j=A,B} \sum_{p=1}^{P} \left(\sigma_j^\dagger a_{n_p^j} + a_{n_p^j}^\dagger \sigma_j \right), \quad (1)$$

where $\sigma_j^\dagger$ and σ_j are raising and lowering operators for atom j, and $a_n^\dagger$, a_n are bosonic creation and annihilation operators at site n.

Here, we stress that, in a purely photonic 1D lattice with periodic boundary conditions, a global gauge transformation could, in principle, remove the complex hopping phase ϕ from nearest-neighbor couplings. However, in our open-boundary setup with spatially separated emitter–lattice couplings, such a transformation cannot eliminate the physical effects of ϕ. The synthetic gauge field modifies the interference paths between emitter coupling points, and this phase dependence is observable in the self-energy, population dynamics, and entanglement evolution, as will be demonstrated below.

Synthetic gauge fields in photonic lattices can be realized using several experimental approaches. A prominent method involves the temporal modulation of the refractive index or hopping amplitudes [86]. Alternatively, synthetic magnetic fields can emerge in photonic systems through engineered optical paths in arrays of helically curved waveguides [87–89]. Lastly, complex hopping terms of the form of $Je^{\pm i\phi}$ can be formed by coupling resonant cavities with metamaterial interlinks of positive and negative refractive indices [85]. These approaches enable the realization of a nontrivial band topology and chiral light propagation, consistent with the effective model used in this work.

2.2. Schrödinger Equation and Coupled Rate Equations

In the single-excitation subspace, the wavefunction is written as

$$|\psi(t)\rangle = C_A(t)|e_A, g_B, \text{vac}\rangle + C_B(t)|g_A, e_B, \text{vac}\rangle + \sum_n C_n(t)|g_A, g_B, 1_n\rangle, \quad (2)$$

where $|1_n\rangle = a_n^\dagger|\text{vac}\rangle$ denotes a photon localized at site n.

Projecting the Schrödinger equation onto each basis state yields

$$\frac{dC_A(t)}{dt} = -i\Delta C_A(t) - ig\sum_{p=1}^{P} C_{n_p^A}(t), \tag{3}$$

$$\frac{dC_B(t)}{dt} = -i\Delta C_B(t) - ig\sum_{p=1}^{P} C_{n_p^B}(t), \tag{4}$$

$$\frac{dC_n(t)}{dt} = -ig\left(\sum_{p=1}^{P}\delta_{n,n_p^A}C_A(t) + \sum_{p=1}^{P}\delta_{n,n_p^B}C_B(t)\right) + iJ\left(e^{i\phi}C_{n+1}(t) + e^{-i\phi}C_{n-1}(t)\right). \tag{5}$$

These equations describe atomic amplitudes coupled to photonic fields at multiple discrete sites and capture chiral propagation in the lattice.

2.3. Resolvent Method and Self-Energy Matrix

Applying the Laplace transform $\tilde{f}(z) = \int_0^\infty dt\, e^{izt} f(t)$ to the above equations yields a closed system of algebraic equations in the frequency domain. Eliminating the field amplitudes $\tilde{C}_n(z)$ via the lattice Green function,

$$\tilde{C}_n(z) = -ig\left(\sum_{p=1}^{P} G_{n,n_p^A}(z)\tilde{C}_A(z) + \sum_{p=1}^{P} G_{n,n_p^B}(z)\tilde{C}_B(z)\right), \tag{6}$$

and substituting it into the transformed equations for $\tilde{C}_A(z), \tilde{C}_B(z)$ leads to

$$[(z-\Delta)\mathbb{I} - \mathbf{\Sigma}(z)]\begin{pmatrix}\tilde{C}_A(z)\\ \tilde{C}_B(z)\end{pmatrix} = i\begin{pmatrix}C_A(0)\\ C_B(0)\end{pmatrix}, \tag{7}$$

where $\mathbb{I}$ is the 2×2 unity matrix and $\mathbf{\Sigma}(\mathbf{z})$ is the self-energy matrix with elements

$$\Sigma_{AA}(z) = g^2\sum_{p,p'=1}^{P} G(n_p^A - n_{p'}^A; z), \tag{8}$$

$$\Sigma_{BB}(z) = g^2\sum_{p,p'=1}^{P} G(n_p^B - n_{p'}^B; z), \tag{9}$$

$$\Sigma_{AB}(z) = g^2\sum_{p,q=1}^{P} G(n_p^A - n_q^B; z), \tag{10}$$

$$\Sigma_{BA}(z) = g^2\sum_{p,q=1}^{P} G(n_p^B - n_q^A; z). \tag{11}$$

The off-diagonal elements Σ_{AB}, Σ_{BA} represent photon-mediated coherent interactions between the two atoms.

2.4. Evaluation of the Green Function

For a 1D tight-binding lattice with synthetic phase ϕ, the Green function in real space is [84]

$$G(n_p - n_{p'}; (z)) = \int_{-\pi}^{\pi}\frac{dk}{2\pi}\frac{e^{ikr}}{z + 2J\cos(k+\phi)} = \frac{(-\chi)^{|n_p - n_{p'}|}}{\sqrt{z^2 - 4J^2}}, \tag{12}$$

where, for $\mathrm{Re}\, z \gtrless 0$,

$$\chi_\pm = \left(\frac{-z \pm \sqrt{z^2 - 4J^2}}{2J}\right)e^{i\phi}. \tag{13}$$

This expression enables the analytical evaluation of all self-energy terms by summing over the spatial separations between coupling points. In particular, the cross terms $\Sigma_{AB}(z)$

$$\Sigma_{AB}(z) = \frac{g^2}{\sqrt{z^2 - 4J^2}} \sum_{p,q=1}^{P} (-\chi)^{|n_p^A - n_q^B|}, \tag{14}$$

capture interference across the P^2 pathways between the two atoms, since the relative separations $|n_p^A - n_q^B|$ include all combinations of coupling site differences between atoms A and B.

We assume that all coupling points are equidistant and separated by distance d. For a braided configuration of the two GAs, see Figure 1. Equation (14) becomes

$$\Sigma_{AB}(z) = \frac{g^2}{\sqrt{z^2 - 4J^2}}[(-\chi)^{3d} + 3(-\chi)^{d}], \tag{15}$$

We stress that the photonic lattice acts as a structured reservoir for the emitters, enabling dissipation and memory effects without requiring an additional external bath. Although the global dynamics are unitary and the system is at zero temperature, the emitter subsystem exhibits irreversible behavior due to coupling to the photonic continuum. The retarded Green function is defined by the standard analytic continuation $\omega \to \omega + i\epsilon$, ensuring well-posedness and causality.

2.5. Bound States and Non-Markovian Dynamics

The resolvent formalism reveals that the atomic dynamics are governed by the poles of the Laplace-transformed evolution operator, which are the solutions to the characteristic equation

$$\det[(z - \Delta)\mathbb{I} - \Sigma(z)] = 0. \tag{16}$$

These poles determine the long-time behavior of the system, as they correspond to the eigenmodes of the hybridized atom–field system [16]. In structured reservoirs such as tight-binding photonic lattices, poles may emerge both outside and inside the band, depending on the interference conditions and coupling geometry.

For two identical giant atoms (GAs), the dynamics can be decomposed into symmetric and antisymmetric excitation sectors using the collective states [16]

$$|\pm\rangle = \frac{1}{\sqrt{2}}(|e_A, g_B\rangle \pm |g_A, e_B\rangle).$$

Each sector evolves independently under an effective Green function,

$$G_{\pm}(z) = \frac{1}{z - \Delta - \Sigma_{\pm}(z)}, \qquad \Sigma_{\pm}(z) = \Sigma_{AA}(z) \pm \Sigma_{AB}(z), \tag{17}$$

where $\Sigma_{AA}(z)$ is the local self-energy, and $\Sigma_{AB}(z)$ captures photon-mediated interactions between the atoms. Due to the spatial structure of $\Sigma_{AB}(z)$, the poles of $G_+(z)$ and $G_-(z)$ typically occur at different locations in the complex plane, even when the atoms are identical. This splitting of symmetric and antisymmetric bound states reflects the collective, nonlocal nature of giant atom interactions in structured baths.

By identifying and classifying the poles of $G_{\pm}(z)$, one can characterize conventional bound states but also quasi-bound states with small imaginary parts, corresponding to long-lived collective excitations. These features are inherently non-Markovian, stemming from time-delayed feedback, energy-dependent self-energy structure, and nonlocal interference. Although the real-frequency poles identified here do not meet the formal criterion for a bound state in the continuum involving a pole-zero cancellation [90], they correspond to

non-decaying emitter–field eigenstates with suppressed coupling to the continuum. These states underlie the long-lived coherence and entanglement plateaus observed below. Generally, the pole structure of the resolvent serves as a tool in understanding and engineering entangled steady states and decoherence-free interactions in extended quantum systems.

3. Results and Discussion

3.1. Bound States

Figure 2 shows the complex poles of the Laplace-transformed dynamics for four different values of the synthetic phase ϕ. Each panel corresponds to a fixed ϕ and displays the symmetric (G_+) and antisymmetric (G_-) poles. These poles are obtained as solutions to the bound-state equations $z - \Delta - \Sigma_\pm(z) = 0$, with $\Delta = 0$ and a braided coupling configuration.

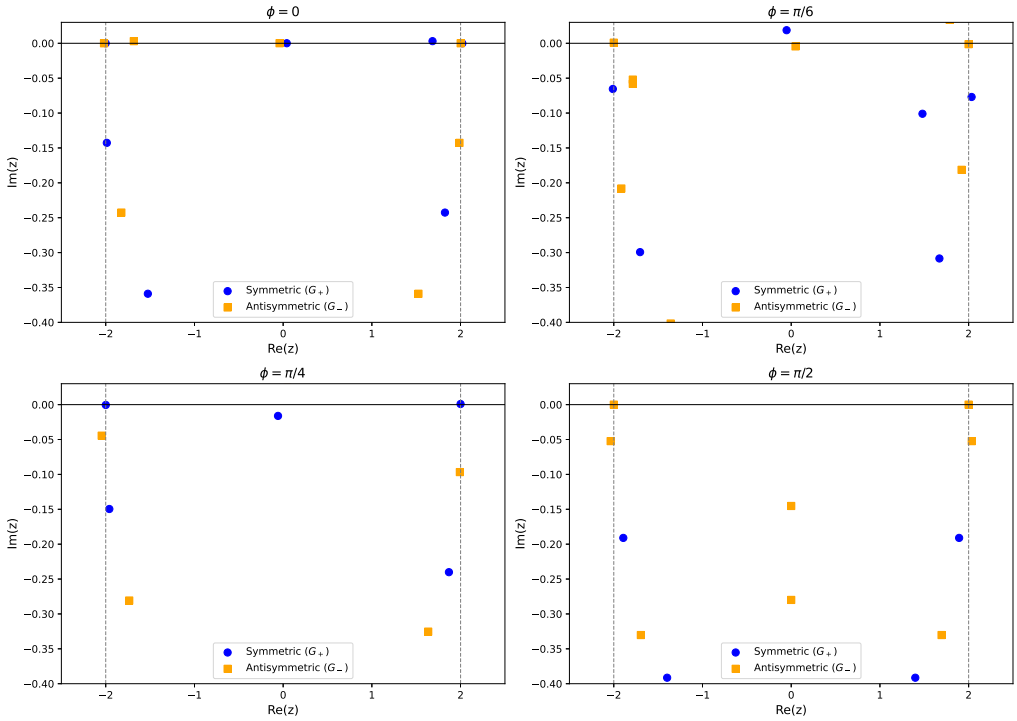

Figure 2. Complex poles of the resolvent $G_\pm(z)$ for two braided giant atoms with separation $d = 5$, zero detuning ($\Delta = 0$), and various values of the synthetic phase $\phi = 0, \pi/6, \pi/4, \pi/2$. The symmetric and antisymmetric poles are shown in blue and orange, respectively. Vertical dashed lines indicate the photonic band edges at $\pm 2J$. Bound states appear as real poles (negligible imaginary part) within the band, while complex poles represent quasi-bound states with finite decay rates.

Across all values of ϕ, we observe the appearance of two categories of collective modes. The first consists of bound states, which are resolvent poles with strictly real energies inside the photonic band. These states are non-radiative and result from perfect destructive interference between the multiple coupling paths of the two giant atoms. Their spectral positions and symmetry classification vary with ϕ, showing that the synthetic phase modulates the interference conditions necessary for bound-state formation. The second category consists of quasi-bound states with small imaginary parts, corresponding to slowly decaying modes. These arise when interference is incomplete, allowing residual coupling to the photonic lattice. The phase dependence of the resolvent poles highlights the versatility of giant atoms in structured environments. By tuning ϕ, one can continuously control the formation and spectral location of bound states, modulate decay channels, and engineer robust, long-lived collective excitations. These results demonstrate the potential

of synthetic gauge fields in enabling non-Markovian quantum control through geometry and interference [16,84].

3.2. Population Dynamics

Figure 3 displays the time evolution of the excited-state populations $|C_A(t)|^2$ and $|C_B(t)|^2$ of the two braided giant atoms of Figure 1. The system is initialized with atom A excited and atom B in the ground state, and the atomic detuning is fixed at $\Delta = 0$, placing the transition frequency at the center of the photonic band. The dynamics are shown for four distinct values of the synthetic gauge phase $\phi = 0, \pi/6, \pi/4, \pi/2$, which modulates the directionality of photon propagation in the lattice. The coupling strength is fixed at $g = 0.2$, consistent with previous works [16,84].

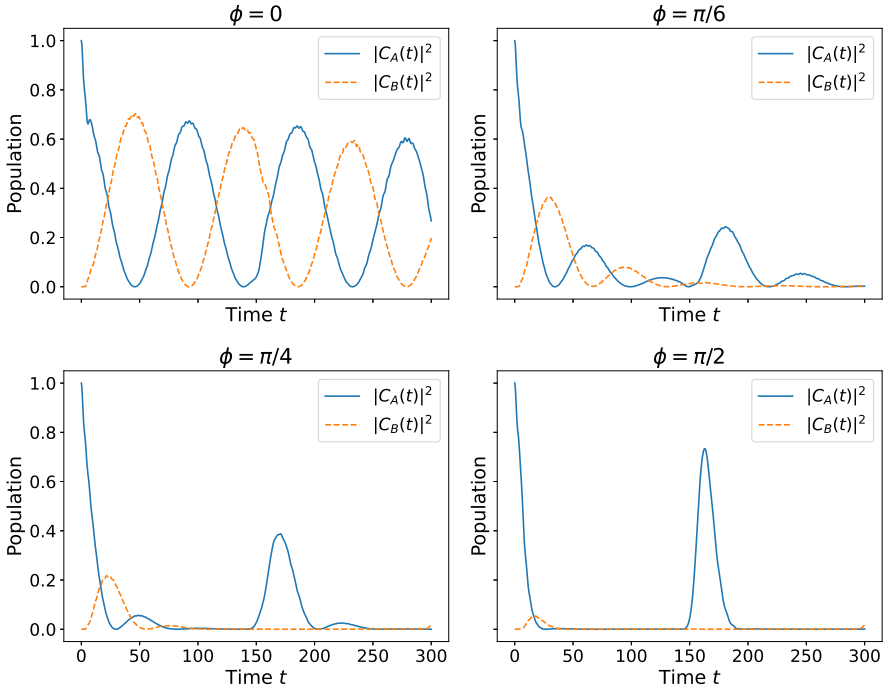

Figure 3. Time evolution of the populations $|C_A(t)|^2$ and $|C_B(t)|^2$ for two giant atoms in a braided configuration coupled to a one-dimensional photonic lattice. Each subplot corresponds to a different value of the synthetic phase $\phi = 0, \pi/6, \pi/4, \pi/2$. The detuning is fixed at $\Delta = 0$, and the system is initialized with atom A in the excited state.

For $\phi = 0$, the excited-state population of atom A exhibits coherent oscillations between the two atoms, characteristic of decoherence-free interaction (DFI). In this regime, the initial excitation is not dissipated into the lattice but rather undergoes coherent exchange between the emitters. This behavior arises from the perfect destructive interference of emission pathways due to the symmetric braided coupling geometry. This symmetry leads to the cancellation of the dissipative components of the self-energy, leaving only the coherent exchange term [16]. The nearly complete absence of population decay in this case indicates the formation of a decoherence-free subspace, where the system evolution is governed by reversible dynamics despite being embedded in a continuum.

As the phase ϕ is varied away from zero, the destructive interference between the different coupling paths becomes imperfect. At $\phi = \pi/6$ and $\pi/4$, the oscillations become damped, and, at $\phi = \pi/2$, they are almost entirely suppressed. The population decays rapidly into the photonic bath, with only a small residual excitation persisting. This behavior reflects the loss of DFI and the onset of non-Markovian dissipation, consistent with the structure of the phase-dependent self-energy $\Sigma(z)$ [84]. The gauge phase ϕ modifies the

relative phase between the different emission pathways, altering the interference condition and allowing part of the atomic excitation to escape into the lattice.

The coherent oscillations observed for $\phi = 0$ are determined by the real part of the difference between the symmetric and antisymmetric collective modes of the system. Their decay envelopes, which are only weakly present in this case, originate from the small imaginary parts of the corresponding poles of the Laplace-transformed amplitude (see Figure 2). These poles lie close to the real axis but within the complex band continuum, indicating the presence of quasi-bound states with long lifetimes. As ϕ increases toward $\pi/2$, the poles shift deeper into the complex plane, reducing their lifetime and leading to fast irreversible decay.

The presence of population revivals at intermediate times—most prominent for $\phi = 0$ and partially visible for $\phi = \pi/6$ and $\pi/4$—indicates that the dynamics are non-Markovian, with the system retaining memory of its past evolution. These revivals are signatures of the coherent backflow of information from the photonic reservoir into the atomic subsystem, which is characteristic of structured environments with long-lived correlations.

From a physical perspective, the initial decay of atom A corresponds to spontaneous emission into the photonic lattice, followed by interference-induced memory effects due to the spatially separated coupling points. The time required for this interference to build up is related to the internal delay time $\tau \sim d/v_g$, where $v_g = \partial_k \omega(k)$ is the group velocity of the photonic modes [16]. After this delay, if the interference conditions are favorable—as is the case for $\phi = 0$—the excitation becomes confined within the atomic subspace. Otherwise, it radiates irreversibly into the bath.

Figure 4 presents the time evolution of the excited-state populations $|C_A(t)|^2$ and $|C_B(t)|^2$ for detuning $\Delta = -1$, which lies within the photonic band but away from its center. As in the previous case, the system is initialized with atom A excited and atom B in the ground state. Again, four synthetic gauge phases $\phi = 0, \pi/6, \pi/4, \pi/2$ are considered.

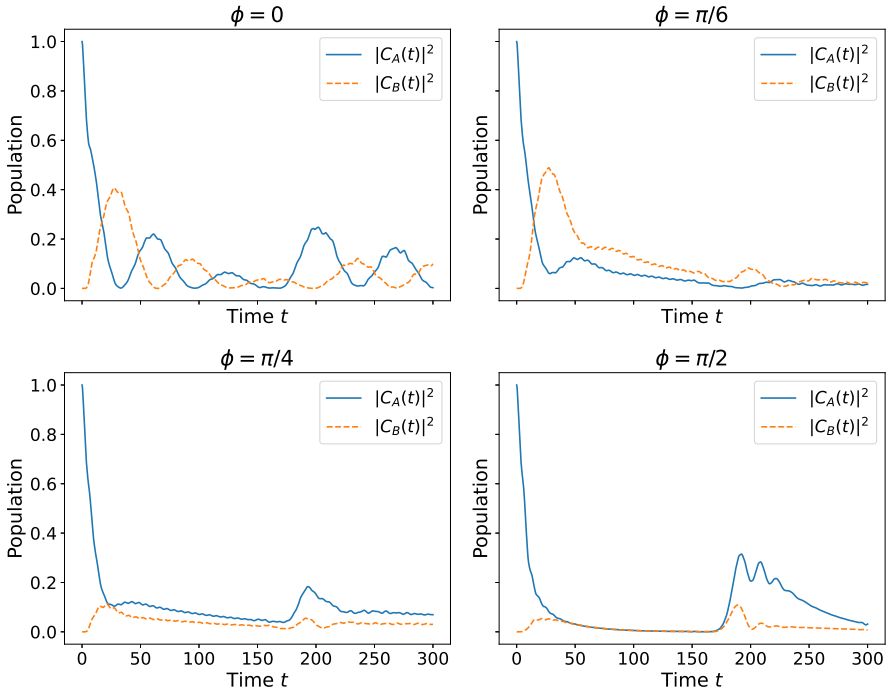

Figure 4. The same as Figure 3 but for $\Delta = -1$.

In the subplot corresponding to $\phi = 0$, we observe coherent population oscillations between the two atoms. However, unlike the perfectly symmetric $\Delta = 0$ case, the oscillations here exhibit visible damping over time, indicating that the destructive interference condi-

tion underlying DFI is partially degraded. This arises because the frequency of the emitter no longer lies at the symmetric center of the band, resulting in asymmetric contributions from the left- and right-propagating photonic modes. The excitation thus undergoes partial leakage into the reservoir, despite an initially coherent exchange.

For $\phi = \pi/6$, this damping becomes more pronounced. The initial coherent transfer from atom A to atom B is still visible, but the amplitude of the oscillations quickly decreases. The system no longer benefits from the full protection of the DFI regime, and non-Markovian dissipation into the structured reservoir begins to dominate the dynamics.

At $\phi = \pi/4$, the excitation decay becomes even faster, and oscillations are strongly suppressed. While the system still shows a small population bump in atom B following initial emission from atom A, this energy is not coherently exchanged back. The loss channel becomes dominant, and the photonic lattice acts effectively as an absorbing environment. A similar picture is also observed for $\phi = \pi/2$. Overall, even a moderate shift from the band center ($\Delta = -1$) leads to the visible degradation of the coherence observed at $\Delta = 0$, and this effect becomes increasingly pronounced as ϕ increases. The suppression of revivals and the enhancement of dissipation suggest that the DFI in the braided geometry is highly sensitive to both the spectral and phase conditions of the environment.

Figure 5 shows the time evolution of the populations $|C_A(t)|^2$ and $|C_B(t)|^2$ for detuning $\Delta = -2$, corresponding to the lower edge of the photonic band. This spectral position significantly modifies the density of available photonic modes and induces nontrivial non-Markovian dynamics due to critical slowing down of the group velocity and localization near the band edge. Similar behavior is observed for the case of $\phi = \pi/4$.

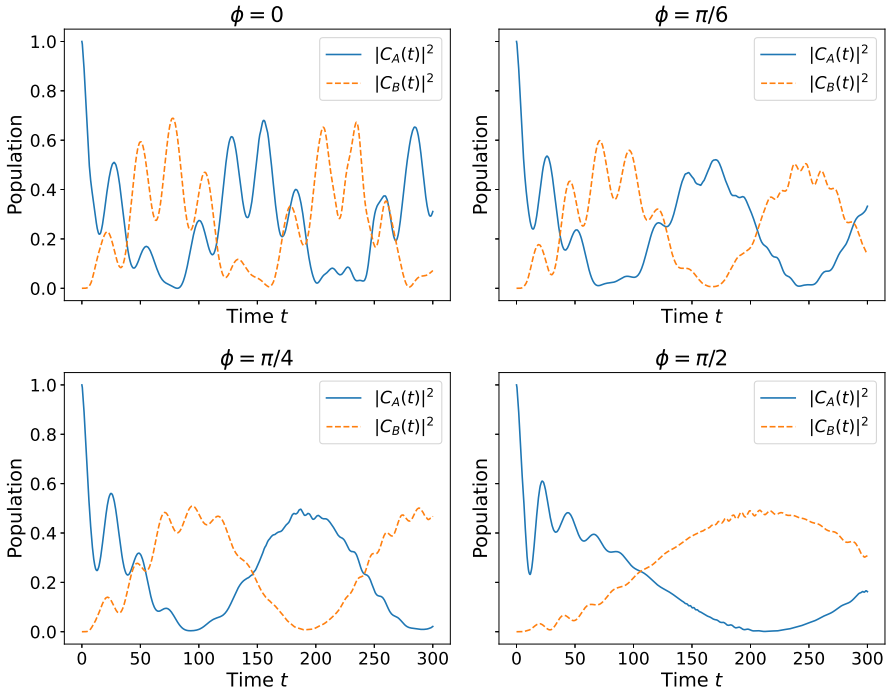

Figure 5. The same as Figure 3 but for $\Delta = -2$.

For $\phi = \pi/6$, these long-lived oscillations persist but show signs of gradual damping. The interference becomes slightly imperfect due to the gauge phase, allowing limited dissipation into the bath. However, population revivals and the substantial occupation of both atoms remain evident. The interaction remains largely reversible, showing signatures of partial decoherence-free dynamics, enabled by the proximity to the band edge.

In the $\phi = \pi/4$ subplot, we observe the stronger damping of the coherent exchange and a more pronounced population decay. While the group velocity is still suppressed, the

interference pattern no longer supports a robust decoherence-free state. The presence of a phase mismatch leads to a small but nonzero imaginary component in the self-energy, which enables slow leakage into the continuum. Nevertheless, weak revivals are still visible, reflecting long-lived photonic correlations.

At $\phi = \pi/2$, the population decay becomes more rapid, and the revival behavior is largely suppressed. Although $\Delta = -2$ places the system at the band edge, the destructive interference conditions are maximally broken here. The excitation is no longer confined, and the slow leakage of the population becomes a dominant feature. The system demonstrates non-exponential decay due to the vanishing density of states near the band edge, but without strong coherent feedback between the atoms.

Overall, we observe an interplay between the spectral location (at the band edge) and synthetic gauge-induced interference. The vanishing group velocity near the edge naturally leads to suppressed decay and enhanced non-Markovianity, while the gauge phase ϕ controls whether this non-Markovian behavior results in revival or dissipation.

Figure 6 shows the excited-state population dynamics $|C_A(t)|^2$ and $|C_B(t)|^2$ for two braided giant atoms coupled to a one-dimensional photonic lattice with detuning $\Delta = -3$, placing the atomic frequency outside the photonic band. In this regime, the lattice supports no resonant propagating modes, and emission into the continuum is forbidden. The coupling instead leads to the formation of exponentially localized bound states.

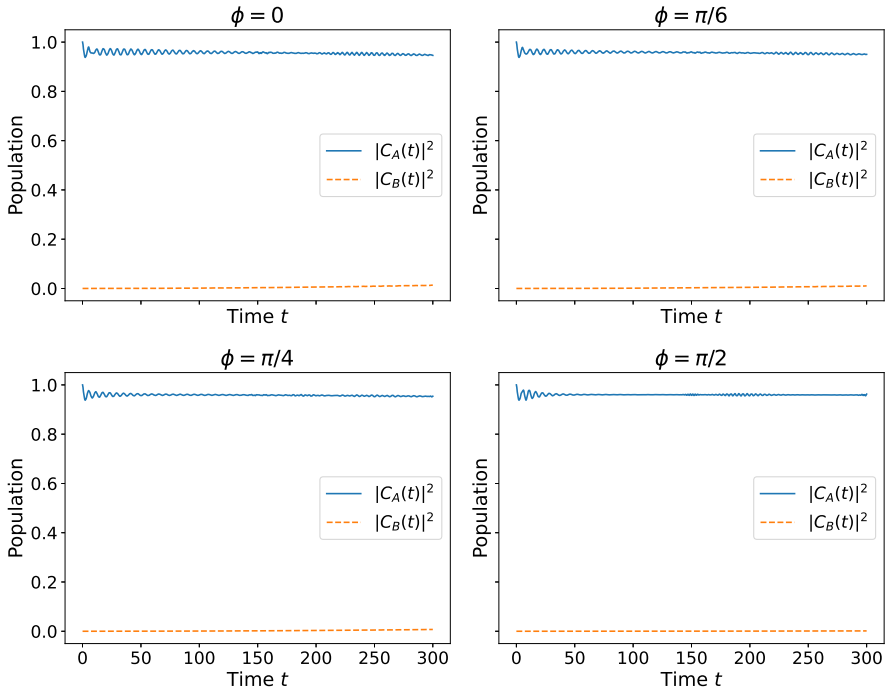

Figure 6. The same as Figure 3 but for $\Delta = -3$.

Across all values of the synthetic gauge phase $\phi = 0, \pi/6, \pi/4, \pi/2$, the population of atom A remains effectively constant, with no significant decay or transfer to atom B. This behavior confirms that the excitation is trapped in a bound state and isolated from the reservoir. The absence of oscillations or leakage reflects the lack of photonic density of states at the detuned frequency. Even when ϕ introduces phase asymmetry, as in $\phi = \pi/6$ and $\pi/4$, or maximally breaks interference at $\phi = \pi/2$, the dynamics remain frozen. The gauge field has no effect outside the band, where the system is spectrally decoupled. The braided configuration plays no role in this nonradiative regime, and the bound state remains robust against phase variations.

This figure complements earlier results for $\Delta = 0, -1, -2$, illustrating a clear transition: from coherent exchange ($\Delta = 0$), to partial damping ($\Delta = -1$), to inhibited decay and revivals at the band edge ($\Delta = -2$), and finally to complete localization ($\Delta = -3$). These results demonstrate how spectral detuning and synthetic gauge control together enable fine tuning between coherent, dissipative, and localized regimes in giant atom systems coupled to structured photonic lattices.

3.3. Atom–Field Entanglement and Entropy Dynamics

Figure 7 shows the time evolution of the von Neumann entropy $S(t)$ for two braided giant atoms interacting with a structured photonic lattice (see Appendix A). The entropy is computed from the reduced atomic density matrix by tracing out the photonic modes and serves as a measure of atom–field entanglement (see Appendix A). Each subplot corresponds to a fixed detuning value $\Delta = 0, -1, -2, -3$, with curves shown for four values of the synthetic gauge phase $\phi = 0, \pi/6, \pi/4, \pi/2$.

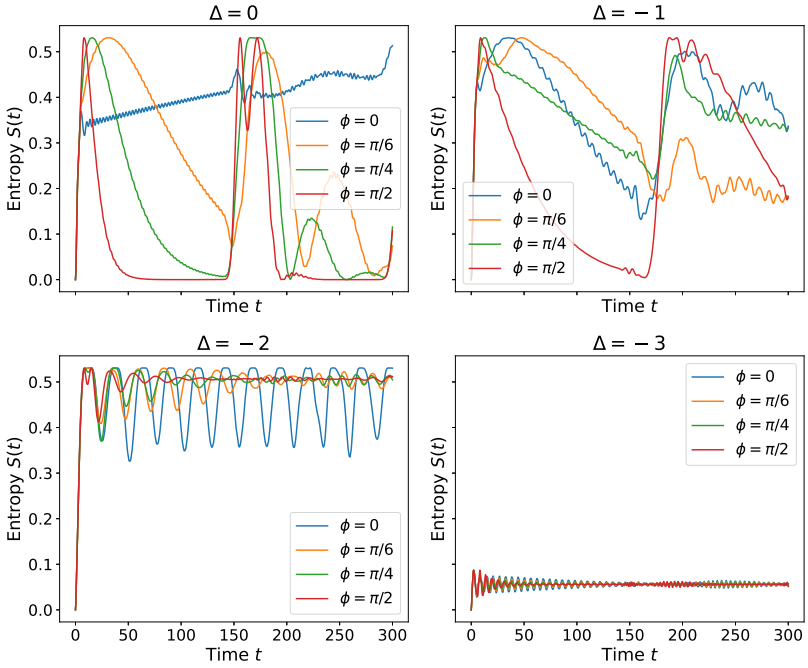

Figure 7. Time evolution of the von Neumann entropy $S(t)$ for two giant atoms coupled to a one-dimensional photonic lattice, shown for four detunings $\Delta = 0, -1, -2, -3$. Each subplot corresponds to a different Δ, and, within each, curves for $\phi = 0, \pi/6, \pi/4, \pi/2$ are shown.

At $\Delta = 0$, the entropy dynamics exhibit strong dependence on the synthetic phase ϕ. For $\phi = 0$, the entropy remains confined to a narrow range of low values throughout the evolution, reflecting sustained coherence and weak entanglement with the photonic field. This behavior is consistent with the presence of a decoherence-free subspace enabled by destructive interference. In contrast, for $\phi = \pi/6, \pi/4$, and $\pi/2$, the entropy shows pronounced non-monotonic variations, with recurrent rises and drops over time. These fluctuations indicate cycles of entanglement generation and partial recoherence, characteristic of non-Markovian dynamics where the excitation temporarily leaves and then returns to the atomic subsystem. The absence of true saturation in these cases highlights the dynamic interplay between atom–field coupling and interference conditions. Similar behavior is observed for $\Delta = -1$.

At the band edge ($\Delta = -2$), the entropy dynamics clearly reflect the emergence of strong non-Markovian behavior. For $\phi = 0$, the entropy rapidly rises to a near-maximal value and exhibits sustained, large-amplitude oscillations around it, indicating persistent

recoherence and the recurrent exchange of excitation between the atoms and the field. This is consistent with the near-zero group velocity at the band edge, which supports photon trapping and delayed feedback. In general, the non-monotonic behavior of the von Neumann entropy indicates the non-Markovian character of the dynamics. Due to the structured reservoir and chiral couplings, the system retains memory and exhibits partial reversibility, leading to periodic entanglement revivals rather than thermal relaxation.

For $\phi = \pi/6$ and $\pi/4$, similar qualitative behavior is observed, although the entropy oscillations are significantly smoother and more damped, suggesting reduced but still non-negligible memory effects. The fluctuations remain around a high baseline entropy value, indicating a sustained but partially decohered entangled state. Even at $\phi = \pi/2$, where chirality suppresses feedback most effectively, the entropy still rises slowly and saturates with minor fluctuations, pointing to the overall suppression—but not elimination—of entanglement backflow due to the proximity to the band edge.

For $\Delta = -3$, outside the photonic band, the entropy remains near zero for all values of ϕ. This confirms that the system forms photonic bound states, with the atomic excitation trapped and decoupled from the reservoir. With no accessible modes for emission or exchange, the atomic subsystem evolves as an effectively closed system, maintaining purity and avoiding entanglement with the environment.

3.4. Atomic Entanglement and Concurrence Dynamics

Figure 8 shows the time evolution of the concurrence $C(t)$ between the two giant atoms of Figure 1. The concurrence is computed from the reduced atomic density matrix and quantifies the degree of two-qubit entanglement (see Appendix B). Each panel corresponds to a fixed detuning value $\Delta = 0, -1, -2, -3$, while each curve within a panel represents a different value of the synthetic gauge phase $\phi = 0, \pi/6, \pi/4, \pi/2$.

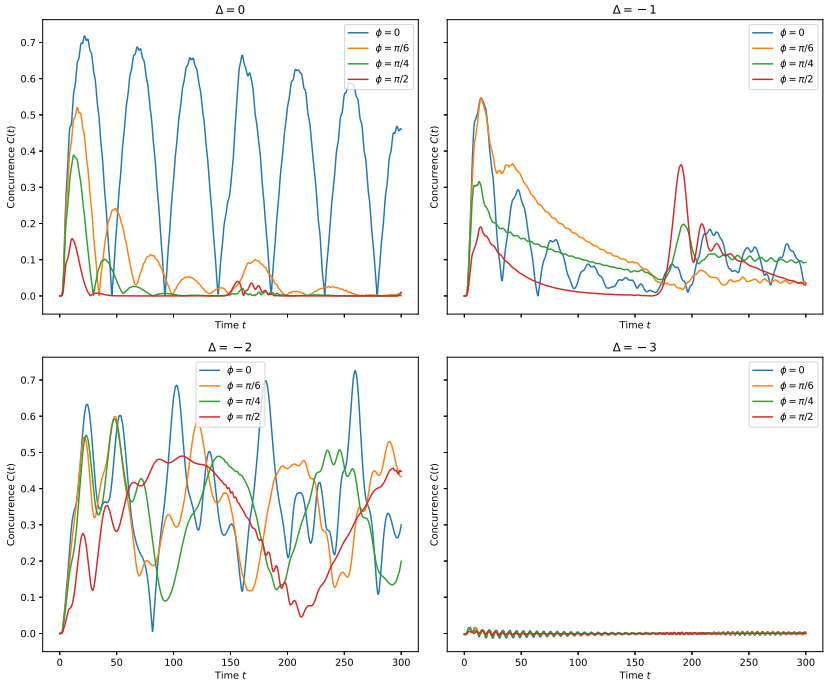

Figure 8. Time evolution of the concurrence $C(t)$ between two giant atoms coupled to a one-dimensional photonic lattice. Each subplot corresponds to a fixed detuning value $\Delta = 0, -1, -2, -3$, and, within each panel, curves for $\phi = 0, \pi/6, \pi/4, \pi/2$ are shown.

For $\Delta = 0$, concurrence exhibits strong oscillations for $\phi = 0$, consistent with coherent excitation exchange and reversible entanglement generation. These oscillations are long-lived and regular, indicating that the atoms periodically become maximally entan-

gled before returning to separable states. For intermediate phases ($\phi = \pi/6, \pi/4$), the oscillations become damped, and concurrence partially decays but can revive due to non-Markovian feedback. For $\phi = \pi/2$, entanglement is strongly suppressed, with concurrence quickly decaying to near zero.

At $\Delta = -1$, the concurrence behavior becomes less oscillatory and more damped overall. For $\phi = 0$, there are still visible peaks in $C(t)$, but they decay more quickly than at resonance. Intermediate phases produce delayed or attenuated revivals, and $\phi = \pi/2$ again results in fast entanglement loss. This shift reflects the reduced density of photonic modes and the corresponding weakening of coherent interactions.

At the band edge detuning $\Delta = -2$, the concurrence dynamics exhibit pronounced signatures of non-Markovian behavior across all values of the synthetic phase ϕ. For $\phi = 0$, the concurrence displays high-amplitude, low-frequency oscillations that persist throughout the simulation window. These sustained revivals reflect the partial localization of excitation and the back-and-forth exchange of the population between the two atoms, consistent with the presence of quasi-bound states and a suppressed group velocity at the band edge. For intermediate values $\phi = \pi/6$ and $\pi/4$, the concurrence retains similar revival-like features, although the oscillations are smoother and slightly damped, suggesting partial delocalization and weaker atom–atom feedback. Notably, the concurrence remains finite for extended durations, indicating long-lived quantum correlations. In the case of $\phi = \pi/2$, although the concurrence magnitude is somewhat reduced compared to $\phi = 0$, it still exhibits visible oscillatory behavior rather than flat decay. These persistent fluctuations suggest that, even under maximum synthetic chirality, the proximity to the band edge inhibits complete decoherence, maintaining a degree of entanglement.

For $\Delta = -3$, which lies outside the photonic band, concurrence remains effectively zero throughout the evolution, regardless of ϕ. Since the excitation is confined to photonic bound states and cannot be exchanged between the atoms, no entanglement is generated. The atoms evolve independently, and the concurrence vanishes at all times, consistent with the frozen population dynamics observed in previous figures.

Overall, the concurrence results confirm that both spectral detuning and synthetic phase ϕ serve as powerful tools for the tuning of entanglement generation, revival, and decay in structured photonic environments. While the presence of DFI enables periodic entanglement at $\Delta = 0$, detuning toward the band edge shifts the dynamics toward slower, revival-driven entanglement. Deep in the gap, interaction is completely suppressed, and the atomic subsystems remain separable. This highlights the essential role of the band structure and synthetic chirality in engineering quantum correlations in lattice-coupled giant atom systems.

Figure 9 shows the time evolution of the concurrence $C(t)$ when the two giant atoms are initially prepared in the symmetric Bell state $(|eg\rangle + |ge\rangle)/\sqrt{2}$, contrasting with the single-excitation case presented in Figure 8. We note that initializing the two giant atoms in a Bell state allows us to directly track how entanglement is preserved or degraded during non-Markovian evolution in a structured photonic reservoir. If the concurrence $C(t)$ remains near 1, the entanglement is robust, often due to bound states or interference effects that suppress decoherence. The rapid decay of $C(t)$ signals entanglement loss from radiative leakage. Intermediate cases, where $C(t)$ oscillates, indicate partial recoherence and memory effects, reflecting periodic entanglement revival driven by atom–field backaction.

At $\Delta = 0$, the Bell state remains almost robust for $\phi = 0$, with the slow decay of concurrence due to interference-protected dynamics—similar to the recurrent entanglement generation observed in the single-excitation case. However, for a larger ϕ, the Bell state exhibits a more pronounced and irreversible entanglement loss, highlighting its vulnerability to synthetic asymmetry even without requiring excitation exchange.

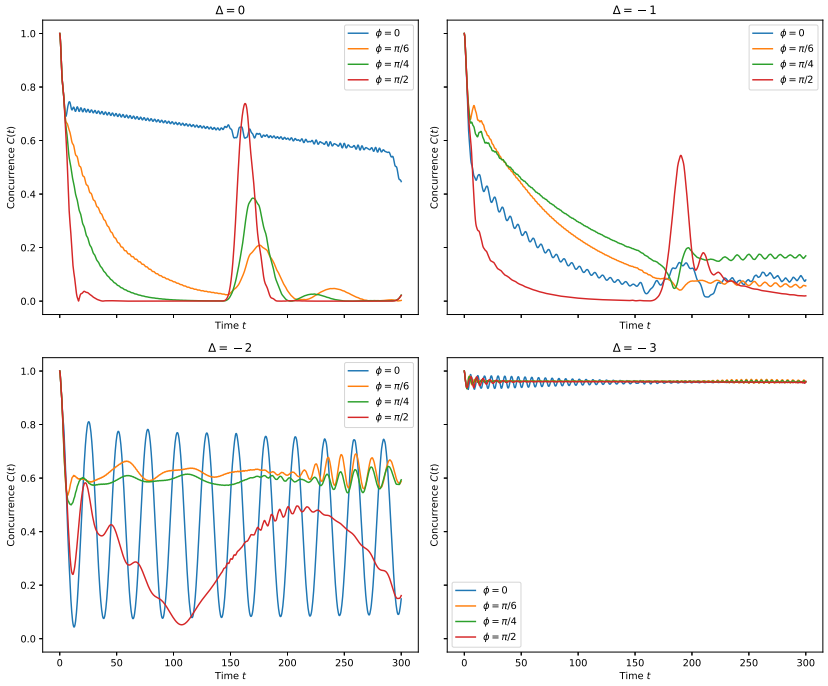

Figure 9. The same as Figure 8 but for two giant atoms initially prepared in the symmetric Bell state $(|eg\rangle + |ge\rangle)/\sqrt{2}$.

For $\Delta = -1$, the concurrence decays more slowly compared to on-resonant cases, indicating a diminished density of states in the photonic bath. Notably, for $\phi = \pi/2$, there is a clear temporal window in which entanglement is partially revived, pointing to coherent feedback processes.

At the band edge ($\Delta = -2$), the concurrence dynamics become richer and more structured. For $\phi = 0$, we observe pronounced oscillations of $C(t)$ between nearly zero and values as high as 0.8, highlighting significant non-Markovian recoherence cycles. For intermediate phases $\phi = \pi/6$ and $\pi/4$, the concurrence instead fluctuates mildly around a quasi-stationary level, indicating suppressed emission and the enhanced stability of entanglement. The case $\phi = \pi/2$ features an initial decay followed by a broad revival bump, again reflecting delayed photonic feedback near the band edge. These patterns highlight the persistence of quantum correlations in the presence of band-edge-induced group velocity suppression and quasi-bound photonic modes.

For $\Delta = -3$, where the atomic transition lies well outside the photonic band, the initial Bell-state entanglement is largely preserved across all values of the synthetic phase ϕ. In all cases, the concurrence remains close to its initial maximum value, exhibiting only minor oscillations over time. This behavior confirms the presence of atom–field bound states that prevent energy and coherence leakage into the lattice and preserve the initially prepared nonlocal correlations.

In summary, starting from a maximally entangled state reveals how the photonic structure and gauge phase influence entanglement preservation, not just generation. Compared to the single-excitation scenario, the Bell state emphasizes the protective role of localization and interference, while also exposing the fragility of entanglement to synthetic dissipation when these protections are broken.

4. Conclusions

We have studied the non-Markovian dynamics of two giant atoms coupled to a one-dimensional photonic lattice with synthetic chirality. By systematically varying the atomic detuning Δ and the synthetic gauge phase ϕ, we have revealed how structured

environments enable precise control over decoherence, entanglement, and population exchange. Using a combination of Laplace-domain analysis and time-domain simulations, we have characterized both the long-lived bound states and the transient dynamical features of the system.

Our results show that, at zero detuning ($\Delta = 0$), coherent population exchange and long-lived entanglement are enabled by destructive interference in the braided coupling geometry. This leads to the formation of a decoherence-free subspace where excitation is confined to the atomic degrees of freedom and entropy remains low. As ϕ increases, this symmetry is broken, resulting in progressively stronger entanglement with the field and faster decay.

Moving away from the band center ($\Delta = -1$), we observe the partial inhibition of decay and delayed entanglement revival, reflecting a reduced density of photonic states. At the band edge ($\Delta = -2$), non-Markovian dynamics become dominant: population revivals, oscillatory entropy, and long-lived quasi-bound modes emerge due to the vanishing group velocity and formation of near-degenerate pole pairs in the resolvent. For large detuning ($\Delta = -3$), outside the photonic band, both the population dynamics and entanglement are effectively frozen. In this regime, bound states prevent any radiative decay, and the atomic system remains isolated from the environment.

We further contrasted two distinct initializations: one with a single atom excited and one with a symmetric Bell state. While both exhibit similar structural dependences on Δ and ϕ, the Bell-state preparation highlights the dynamics of entanglement degradation and protection. Pre-existing correlations were found to enhance the entanglement robustness within the band and at its edge, but it remains equally vulnerable to asymmetry when interference is broken.

Altogether, our findings demonstrate how synthetic gauge fields and coupling geometry can be exploited to engineer decoherence-free interactions, entangled steady states, and tunable non-Markovian behaviors in quantum photonic platforms. These results offer insight for the design of controllable quantum networks, robust entanglement-preserving interfaces, and synthetic environments for non-Markovian quantum information processing.

Funding: This research received no external funding.

Data Availability Statement: Data are contained within the article.

Conflicts of Interest: The author declares no conflict of interest.

Appendix A. Derivation of the von Neumann Entropy for a Two-Giant-Atom System

We work within the single-excitation subspace, where the state vector of the combined system (atoms + field) can be written as

$$|\Psi(t)\rangle = C_A(t)\,|e,g,0\rangle + C_B(t)\,|g,e,0\rangle + \sum_n C_n(t)\,|g,g,1_n\rangle, \tag{A1}$$

where $|e,g,0\rangle$ and $|g,e,0\rangle$ denote states with one of the atoms excited and the photonic lattice in a vacuum, and $|g,g,1_n\rangle$ corresponds to both atoms in the ground state and a single photon at lattice site n.

To study the entanglement between the two-atom system and the photonic lattice, we compute the von Neumann entropy of the reduced atomic density matrix $\rho_{AB}(t)$, obtained by tracing out the photonic degrees of freedom:

$$\rho_{AB}(t) = \mathrm{Tr}_{\mathrm{field}}\,|\Psi(t)\rangle\langle\Psi(t)|. \tag{A2}$$

Using the orthogonality of the single-photon states with the vacuum and among each other, we obtain

$$\rho_{AB}(t) = \begin{pmatrix} |C_A|^2 & C_A C_B^* \\ C_B C_A^* & |C_B|^2 \end{pmatrix}, \tag{A3}$$

in the basis $\{|e,g\rangle, |g,e\rangle\}$, assuming that the photonic part is traced out. The photon-containing states do not contribute to ρ_{AB} but reduce its norm. Hence, normalization must be performed over the total probability:

$$\mathcal{N}(t) = |C_A(t)|^2 + |C_B(t)|^2 + \sum_n |C_n(t)|^2. \tag{A4}$$

We thus renormalize C_A and C_B as $\tilde{C}_A = C_A/\sqrt{\mathcal{N}}$, $\tilde{C}_B = C_B/\sqrt{\mathcal{N}}$ and compute the normalized reduced density matrix $\tilde{\rho}_{AB}$ using Equation (A3).

The von Neumann entropy is then defined as

$$S(t) = -\mathrm{Tr}[\tilde{\rho}_{AB}(t) \log_2 \tilde{\rho}_{AB}(t)]. \tag{A5}$$

For any 2×2 Hermitian density matrix, the entropy can be evaluated using its eigenvalues $\lambda_{1,2}$. These are

$$\lambda_{1,2}(t) = \frac{1}{2}\left(1 \pm \sqrt{1 - 4\ \det \tilde{\rho}_{AB}(t)}\right). \tag{A6}$$

Finally, the entropy becomes

$$S(t) = -\lambda_1 \log_2 \lambda_1 - \lambda_2 \log_2 \lambda_2. \tag{A7}$$

This expression quantifies the instantaneous atom–field entanglement and is computed at each time step during the simulation.

Appendix B. Concurrence Between Giant Atoms in the Single-Excitation Subspace

For a general two-qubit density matrix ρ, the concurrence is defined as

$$C[\rho] = \max\left\{0, \sqrt{\lambda_1} - \sqrt{\lambda_2} - \sqrt{\lambda_3} - \sqrt{\lambda_4}\right\}, \tag{A8}$$

where λ_i are the eigenvalues (in decreasing order) of the matrix

$$R = \rho\,(\sigma_y \otimes \sigma_y)\,\rho^*\,(\sigma_y \otimes \sigma_y), \tag{A9}$$

and σ_y is the Pauli-Y matrix.

The effective state is a pure (unnormalized) superposition:

$$|\psi_{AB}(t)\rangle = \tilde{C}_A|e,g\rangle + \tilde{C}_B|g,e\rangle. \tag{A10}$$

For a pure state of two qubits in this form, the concurrence reduces to

$$C(t) = 2\,|\tilde{C}_A(t)\tilde{C}_B(t)|. \tag{A11}$$

The concurrence measures strictly the two-atom entanglement, while the von Neumann entropy measures the entanglement of the two-atom system with the rest of the universe (in this case, the photonic field). It is thus possible for the concurrence to vanish (atoms are separable), while the entropy remains finite (due to atom–field entanglement). Conversely, in decoherence-free regimes, the entropy remains small while the concurrence

shows periodic peaks, indicating that the excitation oscillates coherently and entanglement builds up and recedes between the two atoms.

The expression of concurrence directly reveals that maximum entanglement (i.e., $C = 1$) occurs when the two amplitudes have equal magnitude, $|\tilde{C}_A| = |\tilde{C}_B| = 1/\sqrt{2}$, corresponding to a symmetric Bell state,

$$|\Psi(0)\rangle = \frac{1}{\sqrt{2}}(|e,g,0\rangle + |g,e,0\rangle), \tag{A12}$$

where $|e,g,0\rangle$ denotes atom A excited and atom B in the ground state, while $|g,e,0\rangle$ corresponds to atom B excited and atom A in the ground state, both with the photonic field initially in a vacuum. This state represents maximal entanglement between the two atoms. The initial concurrence is given by

$$C(0) = 2\left|\frac{1}{\sqrt{2}} \cdot \frac{1}{\sqrt{2}}\right| = 1, \tag{A13}$$

indicating a perfect quantum correlation.

References

1. Chang, D.E.; Douglas, J.S.; González-Tudela, A.; Hung, C.-L.; Kimble, H.J. Colloquium: Quantum matter built from nanoscopic lattices of atoms and photons. *Rev. Mod. Phys.* **2018**, *90*, 031002. [CrossRef]
2. Sheremet, A.S.; Petrov, M.I.; Iorsh, I.V.; Poshakinskiy, A.V.; Poddubny, A.N. Waveguide quantum electrodynamics: Collective radiance and photon-photon correlations. *Rev. Mod. Phys.* **2023**, *95*, 015002. [CrossRef]
3. Ciccarello, F.; Lodahl, P.; Schneble, D. Waveguide quantum electrodynamics. *Opt. Photonics News* **2024**, *35*, 34. [CrossRef]
4. Hood, J.D.; Goban, A.; Asenjo-Garcia, A.; Lu, M.; Yu, S.P.; Chang, D.E.; Kimble, H.J. Atom–atom interactions around the band edge of a photonic crystal waveguide. *Proc. Natl. Acad. Sci. USA* **2016**, *113*, 10507. https://www.pnas.org/doi/pdf/10.1073/pnas.1603788113. [CrossRef] [PubMed]
5. Owens, J.C.; Panetta, M.G.; Saxberg, B.; Roberts, G.; Chakram, S.; Ma, R.; Vrajitoarea, A.; Simon, J.; Schuster, D.I. Chiral cavity quantum electrodynamics. *Nat. Phys.* **2022**, *18*, 1048–1053. [CrossRef]
6. Scigliuzzo, M.; Calajò, G.; Ciccarello, F.; Perez Lozano, D.; Bengtsson, A.; Scarlino, P.; Wallraff, A.; Chang, D.; Delsing, P.; Gasparinetti, S. Controlling atom-photon bound states in an array of Josephson-junction resonators. *Phys. Rev. X* **2022**, *12*, 031036. [CrossRef]
7. Kim, E.; Zhang, X.; Ferreira, V.S.; Banker, J.; Iverson, J.K.; Sipahigil, A.; Bello, M.; González-Tudela, A.; Mirhosseini, M.; Painter, O. Quantum electrodynamics in a topological waveguide. *Phys. Rev. X* **2021**, *11*, 011015. [CrossRef]
8. Krinner, L.; Stewart, M.; Pazmiño, A.; Kwon, J.; Schneble, D. Spontaneous emission of matter waves from a tunable open quantum system. *Nature* **2018**, *559*, 589–592. [CrossRef]
9. Stewart, M.; Kwon, J.; Lanuza, A.; Schneble, D. Dynamics of matter-wave quantum emitters in a structured vacuum. *Phys. Rev. Res.* **2020**, *2*, 043307. [CrossRef]
10. Kockum, A.F.; Delsing, P.; Johansson, G. Designing frequency-dependent relaxation rates and Lamb shifts for a giant artificial atom. *Phys. Rev. A* **2014**, *90*, 013837. [CrossRef]
11. Vadiraj, A.M.; Ask, A.; McConkey, T.G.; Nsanzineza, I.; Sandbo Chang, C.W.; Frisk Kockum, A.; Wilson, C.M. Engineering the level structure of a giant artificial atom in waveguide quantum electrodynamics. *Phys. Rev. A* **2021**, *103*, 023710. [CrossRef]
12. Frisk Kockum, A.; Johansson, G.; Nori, F. Decoherence-free interaction between giant atoms in waveguide quantum electrodynamics. *Phys. Rev. Lett.* **2018**, *120*, 140404. [CrossRef]
13. Kannan, B.; Ruckriegel, M.J.; Campbell, D.L.; Frisk Kockum, A.; Braumüller, J.; Kim, D.K.; Kjaergaard, M.; Krantz, P.; Melville, A.; Niedzielski, B.M.; et al. Waveguide quantum electrodynamics with superconducting artificial giant atoms. *Nature* **2020**, *583*, 775–779. [CrossRef]
14. Carollo, A.; Cilluffo, D.; Ciccarello, F. Mechanism of decoherence-free coupling between giant atoms. *Phys. Rev. Res.* **2020**, *2*, 043184. [CrossRef]
15. Soro, A.; Frisk Kockum, A. Chiral quantum optics with giant atoms. *Phys. Rev. A* **2022**, *105*, 023712. [CrossRef]
16. Soro, A.; Muñoz, C.S.; Frisk Kockum, A. Interaction between giant atoms in a one-dimensional structured environment. *Phys. Rev. A* **2023**, *107*, 013710. [CrossRef]
17. Du, L.; Guo, L.; Li, Y. Complex decoherence-free interactions between giant atoms. *Phys. Rev. A* **2023**, *107*, 023705. [CrossRef]

18. Guo, L.; Frisk Kockum, A.; Marquardt, F.; Johansson, G. Oscillating bound states for a giant atom. *Phys. Rev. Res.* **2020**, *2*, 043014. [CrossRef]
19. Guo, S.; Wang, Y.; Purdy, T.; Taylor, J. Beyond spontaneous emission: Giant atom bounded in the continuum. *Phys. Rev. A* **2020**, *102*, 033706. [CrossRef]
20. Terradas-Briansó, S.; González-Gutiérrez, C.A.; Nori, F.; Martín-Moreno, L.; Zueco, D. Ultrastrong waveguide QED with giant atoms. *Phys. Rev. A* **2022**, *106*, 063717. [CrossRef]
21. Noachtar, D.D.; Knörzer, J.; Jonsson, R.H. Nonperturbative treatment of giant atoms using chain transformations. *Phys. Rev. A* **2022**, *106*, 013702. [CrossRef]
22. Lim, K.H.; Mok, W.K.; Kwek, L.C. Oscillating bound states in non-Markovian photonic lattices. *Phys. Rev. A* **2023**, *107*, 023716. [CrossRef]
23. Gustafsson, M.V.; Aref, T.; Frisk Kockum, A.; Ekström, M.K.; Johansson, G.; Delsing, P. Propagating phonons coupled to an artificial atom. *Science* **2014**, *346*, 207–211. [CrossRef]
24. Aref, T.; Delsing, P.; Ekström, M.K.; Frisk Kockum, A.; Gustafsson, M.V.; Johansson, G.; Leek, P.J.; Magnusson, E.; Manenti, R. Quantum acoustics with surface acoustic waves. In *Superconducting Devices in Quantum Optics*; Hadfield, R.H., Johansson, G., Eds.; Springer: Berlin, Germany, 2016; pp. 217–244.
25. Manenti, R.; Frisk Kockum, A.; Patterson, A.; Behrle, T.; Rahamim, J.; Tancredi, G.; Nori, F.; Leek, P.J. Circuit quantum acoustodynamics with surface acoustic waves. *Nat. Commun.* **2017**, *8*, 975. [CrossRef]
26. Noguchi, A.; Yamazaki, R.; Tabuchi, Y.; Nakamura, Y. Qubit-assisted transduction for a detection of surface acoustic waves near the quantum limit. *Phys. Rev. Lett.* **2017**, *119*, 180505. [CrossRef] [PubMed]
27. Satzinger, K.J.; Zhong, Y.P.; Chang, H.-S.; Peairs, G.A.; Bienfait, A.; Chou, M.-H.; Cleland, A.Y.; Conner, C.R.; Dumur, É.; Grebel, J.; et al. Quantum control of surface acoustic-wave phonons. *Nature* **2018**, *563*, 661–665. [CrossRef]
28. Moores, B.A.; Sletten, L.R.; Viennot, J.J.; Lehnert, K.W. Cavity quantum acoustic device in the multimode strong coupling regime. *Phys. Rev. Lett.* **2018**, *120*, 227701. [CrossRef]
29. Bolgar, A.N.; Zotova, J.I.; Kirichenko, D.D.; Besedin, I.S.; Semenov, A.V.; Shaikhaidarov, R.S.; Astafiev, O.V. Quantum regime of a two-dimensional phonon cavity. *Phys. Rev. Lett.* **2018**, *120*, 223603. [CrossRef]
30. Sletten, L.R.; Moores, B.A.; Viennot, J.J.; Lehnert, K.W. Resolving phonon fock states in a multimode cavity with a double-slit qubit. *Phys. Rev. X* **2019**, *9*, 021056. [CrossRef]
31. Bienfait, A.; Satzinger, K.J.; Zhong, Y.P.; Chang, H.-S.; Chou, M.-H.; Conner, C.R.; Dumur, É.; Grebel, J.; Peairs, G.A.; Povey, R.G.; et al. Phonon-mediated quantum state transfer and remote qubit entanglement. *Science* **2019**, *364*, 368. [CrossRef]
32. Andersson, G.; Suri, B.; Guo, L.; Aref, T.; Delsing, P. Non-exponential decay of a giant artificial atom. *Nat. Phys.* **2019**, *15*, 1123–1127. [CrossRef]
33. Bienfait, A.; Zhong, Y.P.; Chang, H.-S.; Chou, M.-H.; Conner, C.R.; Dumur, É.; Grebel, J.; Peairs, G.A.; Povey, R.G.; Satzinger, K.J.; et al. Quantum erasure using entangled surface acoustic phonons. *Phys. Rev. X* **2020**, *10*, 021055. [CrossRef]
34. Andersson, G.; Ekström, M.K.; Delsing, P. Electromagnetically induced acoustic transparency with a superconducting circuit. *Phys. Rev. Lett.* **2020**, *124*, 240402. [CrossRef]
35. Joshi, C.; Yang, F.; Mirhosseini, M. Resonance fluorescence of a chiral artificial atom. *Phys. Rev. X* **2023**, *13*, 021039. [CrossRef]
36. González-Tudela, A.; Muñoz, C.S.; Cirac, J.I. Engineering and harnessing giant atoms in high-dimensional baths: A proposal for implementation with cold atoms. *Phys. Rev. Lett.* **2019**, *122*, 203603. [CrossRef]
37. Du, L.; Zhang, Y.; Wu, J.H.; Kockum, A.F.; Li, Y. Giant atoms in a synthetic frequency dimension. *Phys. Rev. Lett.* **2022**, *128*, 223602. [CrossRef]
38. Guimond, P.O.; Vermersch, B.; Juan, M.L.; Sharafiev, A.; Kirchmair, G.; Zoller, P. A unidirectional on-chip photonic interface for superconducting circuits. *npj Quantum Inf.* **2020**, *6*, 32. [CrossRef]
39. Gheeraert, N.; Kono, S.; Nakamura, Y. Programmable directional emitter and receiver of itinerant microwave photons in a waveguide. *Phys. Rev. A* **2020**, *102*, 053720. [CrossRef]
40. Zhang, Y.X.; Carceller, C.R.; Kjaergaard, M.; Sørensen, A.S. Charge-noise insensitive chiral photonic interface for waveguide circuit QED. *Phys. Rev. Lett.* **2021**, *127*, 233601. [CrossRef] [PubMed]
41. Yin, X.-L.; Liu, Y.-H.; Huang, J.-F.; Liao, J.-Q. Single-photon scattering in a giant-molecule waveguide-QED system. *Phys. Rev. A* **2022**, *106*, 013715. [CrossRef]
42. Zhang, Y.; Wang, Y.; Liu, Z.; Li, X.; Chen, H.; Zhou, J.; Zhang, Y.; Liu, Y.; Zhang, L.; Liu, J.; et al. Observation of non-Hermitian skin effect and topology in a non-Hermitian lattice. *Optica* **2022**, *9*, 565–571.
43. Kannan, B.; Almanakly, A.; Sung, Y.; Di Paolo, A.; Rower, D.A.; Braumüller, J.; Melville, A.; Niedzielski, B.M.; Karamlou, A.; Serniak, K.; et al. On-demand directional microwave photon emission using waveguide quantum electrodynamics. *Nat. Phys.* **2023**, *19*, 394. [CrossRef]
44. Wang, Z.Q.; Wang, Y.P.; Yao, J.; Shen, R.C.; Wu, W.J.; Qian, J.; Li, J.; Zhu, S.Y.; You, J.Q. Giant spin ensembles in waveguide magnonics. *Nat. Commun.* **2022**, *13*, 7580. [CrossRef]

45. Guo, L.; Grimsmo, A.L.; Kockum, A.F.; Pletyukhov, M.; Johansson, G. Giant acoustic atom: A single quantum system with a deterministic time delay. *Phys. Rev. A* **2017**, *95*, 053821. [CrossRef]
46. Karg, T.M.; Gouraud, B.; Treutlein, P.; Hammerer, K. Remote Hamiltonian interactions mediated by light. *Phys. Rev. A* **2019**, *99*, 063829. [CrossRef]
47. Ask, A.; Fang, Y.-L.L.; Kockum, A.F. Synthesizing electromagnetically induced transparency without a control field in waveguide QED using small and giant atoms. *arXiv* **2020**, arXiv:2011.15077.
48. Du, L.; Li, Y. Single-photon frequency conversion via a giant Λ-type atom. *Phys. Rev. A* **2021**, *104*, 023712. [CrossRef]
49. Feng, S.L.; Jia, W.Z. Manipulating single-photon transport in a waveguide-QED structure containing two giant atoms. *Phys. Rev. A* **2021**, *104*, 063712. [CrossRef]
50. Cai, Q.Y.; Jia, W.Z. Coherent single-photon scattering spectra for a giant-atom waveguide-QED system beyond the dipole approximation. *Phys. Rev. A* **2021**, *104*, 033710. [CrossRef]
51. Yin, X.-L.; Luo, W.-B.; Liao, J.-Q. Non-Markovian disentanglement dynamics in double-giant-atom waveguide-QED systems. *Phys. Rev. A* **2022**, *106*, 063703. [CrossRef]
52. Gong, Z.; Bello, M.; Malz, D.; Kunst, F.K. Anomalous Behaviors of Quantum Emitters in Non-Hermitian Baths. *Phys. Rev. Lett.* **2022**, *129*, 223601. [CrossRef]
53. Chen, Y.-T.; Du, L.; Guo, L.; Wang, Z.; Zhang, Y.; Li, Y.; Wu, J.-H. Nonreciprocal and chiral single-photon scattering for giant atoms. *Commun. Phys.* **2022**, *5*, 215. [CrossRef]
54. Du, L.; Chen, Y.-T.; Zhang, Y.; Li, Y. Giant atoms with time-dependent couplings. *Phys. Rev. Res.* **2022**, *4*, 023198. [CrossRef]
55. Du, L.; Zhang, Y.; Li, Y. A giant atom with modulated transition frequency. *Front. Phys.* **2023**, *18*, 12301. [CrossRef]
56. Santos, A.C.; Bachelard, R. Generation of maximally entangled long-lived states with giant atoms in a waveguide. *Phys. Rev. Lett.* **2023**, *130*, 053601. [CrossRef]
57. Wang, X.; Zhu, H.-B.; Liu, T.; Nori, F. Realizing quantum optics in structured environments with giant atoms. *Phys. Rev. Res.* **2024**, *6*, 013279. [CrossRef]
58. Zhou, J.; Yin, X.-L.; Liao, J.-Q. Chiral and nonreciprocal single-photon scattering in a chiral-giant-molecule waveguide-QED system. *Phys. Rev. A* **2023**, *107*, 063703. [CrossRef]
59. Gu, W.; Huang, H.; Yi, Z.; Chen, L.; Sun, L.; Tan, H. Correlated two-photon scattering in a one-dimensional waveguide coupled to two- or three-level giant atoms. *Phys. Rev. A* **2023**, *108*, 053718. [CrossRef]
60. Xu, L.; Guo, L. Catch and release of propagating bosonic field with non-Markovian giant atom. *New J. Phys.* **2024**, *26*, 013025. [CrossRef]
61. Longhi, S. Photonic simulation of giant atom decay. *Opt. Lett.* **2020**, *45*, 3017–3020. [CrossRef] [PubMed]
62. Zhao, W.; Wang, Z. Single-photon scattering and bound states in an atom-waveguide system with two or multiple coupling points. *Phys. Rev. A* **2020**, *101*, 053855. [CrossRef]
63. Wang, X.; Liu, T.; Kockum, A.F.; Li, H.-R.; Nori, F. Tunable chiral bound states with giant atoms. *Phys. Rev. Lett.* **2021**, *126*, 043602. [CrossRef]
64. Longhi, S. Rabi oscillations of bound states in the continuum. *Opt. Lett.* **2021**, *46*, 2091–2094. [CrossRef]
65. Yu, H.; Wang, Z.; Wu, J.-H. Entanglement preparation and nonreciprocal excitation evolution in giant atoms by controllable dissipation and coupling. *Phys. Rev. A* **2021**, *104*, 013720. [CrossRef]
66. Vega, C.; Bello, M.; Porras, D.; González-Tudela, A. Qubit-photon bound states in topological waveguides with long-range hoppings. *Phys. Rev. A* **2021**, *104*, 053522. [CrossRef]
67. Smith, A.; Johnson, B.; Lee, C.; Kumar, D.; Nguyen, E.; Patel, F.; Garcia, G.; Chen, H.; Wang, I.; Zhao, J.; et al. Enhanced light–matter interaction in hybrid nanophotonic structures. *Nanophotonics* **2021**, *10*, 567–578.
68. Wang, X.; Li, H.-R. Chiral quantum network with giant atoms. *Quantum Sci. Technol.* **2022**, *7*, 035007. [CrossRef]
69. Xiao, H.; Wang, L.; Li, Z.; Chen, X.; Yuan, L. Bound state in a giant atom-modulated resonators system. *npj Quantum Inf.* **2022**, *8*, 80. [CrossRef]
70. Cheng, W.; Wang, Z.; Liu, Y.X. Topology and retardation effect of a giant atom in a topological waveguide. *Phys. Rev. A* **2022**, *106*, 033522. [CrossRef]
71. Gong, Z.; Bello, M.; Malz, D.; Kunst, F.K. Bound states and photon emission in non-Hermitian nanophotonics. *Phys. Rev. A* **2022**, *106*, 053517 . [CrossRef]
72. Zhang, X.; Cheng, W.; Gong, Z.; Zheng, T.; Wang, Z. Superconducting giant atom waveguide QED: Quantum Zeno and anti-Zeno effects in ultrastrong coupling regime. *arXiv* **2022**, arXiv:2205.03674.
73. Du, L.; Guo, L.; Zhang, Y.; Kockum, A.F. Giant emitters in a structured bath with non-Hermitian skin effect. *Phys. Rev. Res.* **2023**, *5*, L042040. [CrossRef]
74. Du, L.; Chen, Y.-T.; Zhang, Y.; Li, Y.; Wu, J.-H. Decay dynamics of a giant atom in a structured bath with broken time-reversal symmetry. *Quantum Sci. Technol.* **2023**, *8*, 045010. [CrossRef]
75. Bello, M.; Cirac, J.I. Topological effects in two-dimensional quantum emitter systems. *Phys. Rev. B* **2023**, *107*, 054301. [CrossRef]

76. Bag, R.; Roy, D. Quantum light-matter interactions in structured waveguides. *Phys. Rev. A* **2023**, *108*, 053717. [CrossRef]
77. Jia, W.Z.; Yu, M.T. Atom-photon dressed states in a waveguide-QED system with multiple giant atoms. *Opt. Express* **2024**, *32*, 9495–9508. [CrossRef]
78. Gao, Z.-M.; Li, J.-Q.; Li, Z.-W.; Liu, W.-X.; Wang, X. Circuit QED with giant atoms coupling to left-handed superlattice metamaterials. *Phys. Rev. A* **2024**, *109*, 013716. [CrossRef]
79. Zhang, Y.; Liu, X.; Wang, L.; Chen, M.; Zhao, Q.; Li, H. Topological photonics in synthetic dimensions. *Nat. Commun.* **2024**, *15*, 1234. [CrossRef]
80. Leonforte, L.; Sun, X.; Valenti, D.; Spagnolo, B.; Illuminati, F.; Carollo, A.; Ciccarello, F. Quantum optics with giant atoms in a structured photonic bath. *Quantum Sci. Technol.* **2024**, *10*, 015057. [CrossRef]
81. Ingelsten, E.R.; Kockum, A.F.; Soro, A. Avoiding decoherence with giant atoms in a two-dimensional structured environment. *Phys. Rev. Res.* **2024**, *6*, 043222. [CrossRef]
82. Du, L.; Kockum, A.F. Unconventional and robust light–matter interactions based on the non-Hermitian skin effect. *Phys. Rev. Res.* **2025**, *7*, 013140. [CrossRef]
83. Chen, G.; Kockum, A.F. Simulating open quantum systems with giant atoms. *Quantum Sci. Technol.* **2025**, *10*, 025028. [CrossRef]
84. Yannopapas, V. Non-Markovian Dynamics of Giant Atoms Embedded in an One-Dimensional Photonic Lattice with Synthetic Chirality. *Photonics* **2025**, *12*, 527. [CrossRef]
85. Yannopapas, V. Topological zero-dimensional photonic modes in chiral coupled-cavity arrays. *EPJ Quantum Technol.* **2015**, *2*, 6. [CrossRef]
86. Fang, K.; Yu, Z.; Fan, S. Realizing effective magnetic field for photons by controlling the phase of dynamic modulation. *Nat. Photonics* **2012**, *6*, 782–787. [CrossRef]
87. Efremidis, N.K.; Zhang, P.; Chen, Z.; Christodoulides, D.N.; Rüter, C.E.; Kip, D. Wave propagation in waveguide arrays with alternating positive and negative couplings. *Phys. Rev. A* **2010**, *81*, 053817. [CrossRef]
88. Zeuner, J.M.; Efremidis, N.K.; Keil, R.; Dreisow, F.; Christodoulides, D.N.; Tünnermann, A.; Nolte, S.; Szameit, A. Optical analogues for massless Dirac particles and conical diffraction in one dimension. *Phys. Rev. Lett.* **2012**, *109*, 023602. [CrossRef]
89. Longhi, S.; Marangoni, M.; Lobino, M.; Ramponi, R.; Laporta, P.; Cianci, E.; Foglietti, V. Observation of dynamic localization in periodically curved waveguide arrays. *Phys. Rev. Lett.* **2006**, *96*, 243901. [CrossRef]
90. Krasnok, A.; Khurgin, M.; Baranov, D.; Stockman, M.; Alù, A. Anomalies in light scattering. *Adv. Opt. Photonics* **2019**, *11*, 892–951. [CrossRef]